Paper No.
7891

NACE INTERNATIONAL CORROSION 2016 CONFERENCE & EXPO

Effect of monoethylene glycol on sweet top of the line corrosion

Shaoqiang Guo
Institute for Corrosion and Multiphase Technology
Ohio University
342 West State Street
Athens, Ohio 45701
U.S.A

Fernando Farelas
Institute for Corrosion and Multiphase Technology
Ohio University
342 West State Street
Athens, Ohio 45701
U.S.A

Marc Singer
Institute for Corrosion and Multiphase Technology
Ohio University
342 West State Street
Athens, Ohio 45701
U.S.A

ABSTRACT

In wet gas pipelines, Monoethylene glycol (MEG) is a widely used hydrate inhibitor which has been shown to decrease the corrosion rate of carbon steel in CO_2 environments. In a top of the line corrosion (TLC) situation, MEG is also known to affect both water condensation and TLC rates. However, the extent of its effect on corrosion depends mainly on the concentration of MEG present in the condensed water. Until now, rather scarce and conflicting information exist on this topic. This work presents a mechanistic water/MEG co-condensation model in the presence of a noncondensing gas (CO_2). The model predictions of condensation rate and MEG concentration in the condensing phase are compared with loop test results, showing good agreement. The results show that an increase of the MEG content at the bottom of the line decreases the water condensation rate and increases the MEG content of the condensing phase at the top of the line. However, this effect is not significant unless the MEG content in the bulk liquid phase is higher than 70-80 wt%. Long term corrosion experiments are also presented showing that the injection of 50 wt% and 70 wt% MEG at the bottom have a minimal effect on both general and localized corrosion rates. On the other hand, the presence of 90 wt% MEG at the bottom of the line decreased the top of the line corrosion rate significantly due to a sharp decrease in condensation rate and a significant increase in MEG content in the condensing phase.

Key words: top of the line corrosion, monoethylene glycol, carbon dioxide, co-condensation, mechanistic model

INTRODUCTION

For economic reasons and operational flexibility, unprocessed wet gas is often directly transported in subsea pipelines to onshore processing plants for dehydration, rather than being dried on offshore platforms. During wet gas transportation, the water vapor in the gas phase will condense on the internal pipeline surface due to the difference of temperature between the wet gas stream and the outside environment, leading to top of the line corrosion (TLC). TLC is caused by the dissolution of corrosive gases, like carbon dioxide and hydrogen sulfide, in the condensed water. The presence of acetic acid can also enhance TLC. In sweet environment, the initially high rates of iron dissolution lead to the rapid development of a corrosion product layer ($FeCO_3$) on the steel surface. The protectiveness of this layer is constantly challenged by the continuous condensation of water vapor and renewal of water droplets. At low water condensation rates, TLC rates remain manageable. At high water condensation rates, TLC can become a serious issue, leading to pipe failures. The water condensation rate has long been recognized as the key factor influencing the rate of top of the line corrosion in CO_2 environments. In addition, top of the line corrosion can be a serious concern in the oil and gas industry due to the limited options for corrosion mitigation. The traditional corrosion inhibitors injected in the liquid phase at the bottom of the pipeline are often non-volatile and cannot reach the condensed water at the top of the line.

So far, various parameters influencing TLC such as temperature, condensation rate, CO_2 and H_2S partial pressure as well as acetic acid concentration have been extensively investigated.[1-5] Effects of flow velocity, gas pressure and both bulk gas and pipe wall temperature were also studied experimentally and modeling approaches have been proposed.[6,7] However, results on the effect of MEG on top of the line corrosion have been less publicized. MEG is a chemical often injected in subsea wet gas pipeline as a hydrate inhibitor. The subsea wet gas pipelines, with a typical pressure of the order 50-100 bar and gas temperature that can reach close to 4°C in winter, has a potential risk of gas hydrate formation when water is present.[8] Gas hydrates are crystalline compounds consisting of water and light hydrocarbon gases which can plug the pipeline and stop flow.[8] Typically, about 80-90 wt% MEG ('lean MEG') is injected offshore into the pipeline and transferred with water and natural gas. The MEG content in the bottom of the line will be first reduced by mixing with formation water. Further dilution will also occur all along the pipeline due to the condensation of the water vapor from the gas phase. A minimum MEG content of around 40 wt% ('rich MEG') at the onshore end of the pipeline is usually maintained by adjusting the injection rate of MEG at the pipe inlet.[9]

In a number of wet gas pipelines, glycol is also used as a corrosion inhibitor, although it is not its primary function, and a summary of field experiences has been given by Crolet *et. al*.[10] Glycol has a much lower vapor pressure than water, and significantly decreases the water vapor pressure when the water phase contains considerable amount of glycol. Therefore, the injection of glycol in the wet gas pipeline is also expected to lower the water condensation rate and consequently reduce the severity of top of the line corrosion.[11,12] On the other hand, it has been reported that the CO_2 corrosion rate of carbon steel fully immersed in the liquid phase decreases with the increase of glycol concentration.[11,13] An empirical glycol reduction factor developed by de Waard[13] is often used to estimate the inhibition effect of glycol on CO_2 corrosion. The corrosion of X65 steel at various MEG and diethylene glycol (DEG) concentrations was investigated at 25°C and 1 bar CO_2,[14] which included a theoretical description; results showed that the corrosion rates gradually decreased with the increase of glycol concentration, matching the empirical glycol factor. The glycol reduction factor also displayed good agreement with the experimental results at 80°C and 0.56 bar CO_2, but significantly underestimated the corrosion rate at 100°C and 120°C in the presence of 80 wt% MEG at 10 bar of CO_2.[15] The influences of MEG concentration on the CO_2 solubility and diffusivity in the solution as well as the solubility limit of $FeCO_3$ were investigated, but the mechanism of MEG inhibition effect on CO_2 corrosion of carbon steel is still not well understood and no mechanistic model was reported.[14,16-18]

For a better understanding of MEG effects on TLC, it is necessary to have accurate prediction of the co-condensation rate and the MEG concentration in the condensing phase at the top of the line. However, limited information exists on the modeling of MEG and water co-condensation in the literature.[13,19,20]

Available models assume that the MEG/water mixture condensing at the top of line is in equilibrium with the vapor phase without clarifying if the vapor phase is bulk vapor or the vapor in the boundary layers adjacent to the condensed liquid. That information is essential since heat transfer and mass transfer boundary layers exist between the bulk gas phase and condensing aqueous phase. Many results confirmed that the vapor liquid equilibrium actually exists at the liquid vapor interface for multicomponent condensing vapor-gas systems.[21]

In this work, a mechanistic condensation model for the co-condensation of MEG and water is presented based on the water dropwise condensation model developed by Zhang *et. al*.[24] The co-condensation model predicts the overall condensation rate (MEG and water) and the MEG concentration in the condensed liquid phase. The model is verified by comparing with experiments conducted in a large-scale, high-temperature and high-pressure flow loop. Finally, the effect of MEG content at the bottom of the pipeline on the top of the line corrosion rate and localized corrosion is investigated by long term flow loop tests.

MEG/water co-condensation model

It was shown before that the condensation at the top of the pipeline occurs in a dropwise condensation mode rather than a filmwise condensation mode, as became clear from the morphology of corroded steel surface and in situ visual observation.[22-24] In the presence of MEG, evidence of dropwise condensation was confirmed in TLC experiments, and an example is given in Figure 1. It can be seen that the sample surface was occupied by a group of droplets with different diameters ranging from the order of micrometer to millimeter. MEG is miscible with water at any ratio. Therefore, when the water and MEG vapors condense at the top of the pipeline, each condensing droplet will contain a certain amount of MEG. The co-condensation of MEG and water happens when the temperature of the outside environment is low enough to provide an inner pipe temperature below the saturation temperature of the vapor mixture. Such a condition develops concentration and temperature gradients essential for the transfer of both heat and mass.

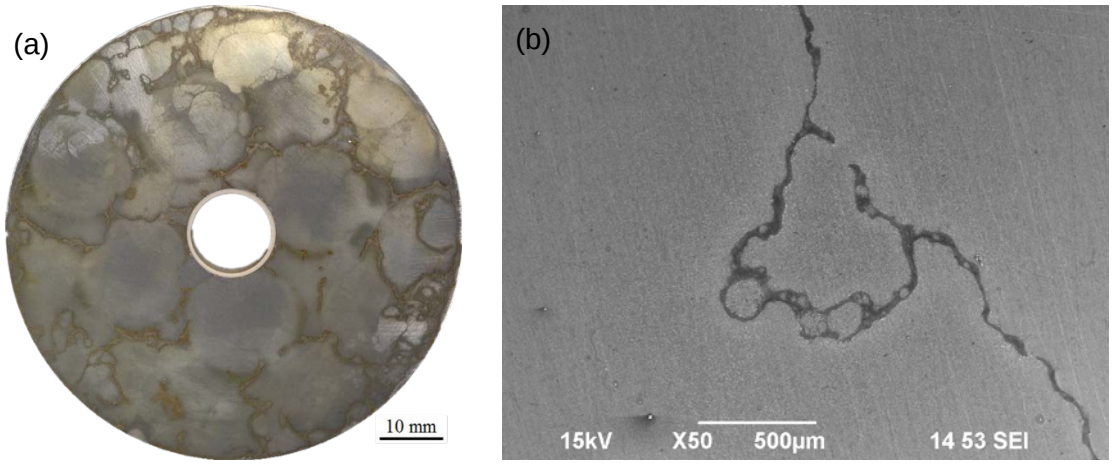

Figure 1: Evidence of dropwise condensation during MEG/water co-condensation (a) sample photo after TLC (b) scanning electron microscope (SEM) image of sample surface.

Zhang *et. al.,*[24] developed a comprehensive review on how to model the heat and mass transfer occurring in dropwise condensation in the presence of non-condensable gases. Only a summary of the modeling

approach is described here, with an emphasis on the notable differences introduced due to the presence of MEG.

Heat balance

A schematic representation of the dropwise co-condensation of MEG and water at the top of the wet gas pipeline and the temperature gradient in a single droplet is shown in Figure 2.

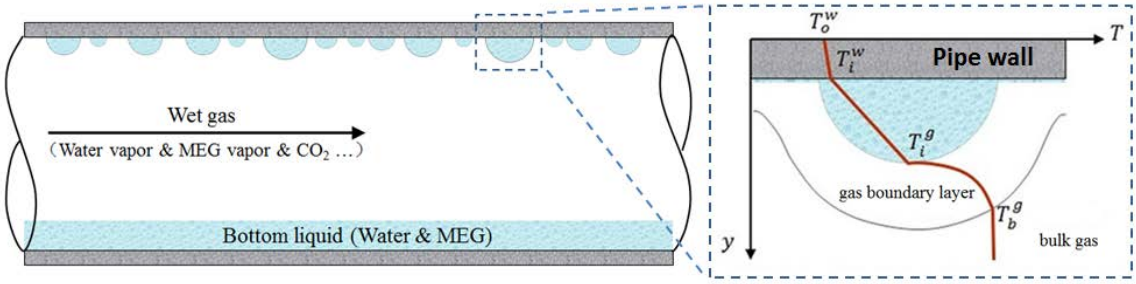

Figure 2: Dropwise condensation of water and MEG at top of the pipeline and temperature gradient in a single condensed droplet. (Adapted from Zhang *et. al.*[24])

In their modeling approach, Zhang *et. al.*[24] included the effect of several key factors, namely the heat transfer through the boundary layer, the phase change at the droplet interface, the influence of the droplet curvature, the heat transfer resistance at the vapor/liquid interface and the heat conduction through the condensed liquid, pipe wall and insulation layer(s).

The total amount of heat is carried from the gas-droplet interface through the condensed liquid droplets and from the pipe wall to the outside environment. Since the pipe wall is covered by a number of droplets of various sizes, the total heat flux (Q) through the droplets has to be calculated through a statistical approach considering the droplet-size distribution N(r).

$$Q = \int_{r_{min}}^{r_{max}} q(r)N(r)dr \quad (1)$$

Where: r_{min} and r_{max} represent the minimum and maximum radii of droplets (m), respectively and q(r) represents the heat flux (W) through a single droplet of radius r.

The total heat flux (Q) between the gas phase to the condensed liquid includes the heat flux through the gas boundary layer (Q_g) and the heat flux released at the droplet interface due to phase change:

$$Q = Q_g + Q_v^{water} + Q_v^{MEG} \quad (2)$$

where: Q_v^{water} and Q_v^{MEG} are the latent heat flux released by the condensation of water and MEG vapors at the droplet interface in W/m^2.

The latent heat flux of Q_v^{water} and Q_v^{MEG} are related to the water and MEG condensation rate, respectively:

$$Q_v^{water} = R_{cond}^{water} H_v^{water} \quad (3)$$

$$Q_v^{MEG} = R_{cond}^{MEG} H_v^{MEG} \quad (4)$$

where R_{cond}^{water} and R_{cond}^{MEG} are water and MEG condensation rate, respectively, in kg/m^2/s; H_v^{water} and H_v^{MEG} are the latent condensation heat for water and MEG, respectively, in J/kg.

The heat flux Q_g through the gas boundary layer to the droplet interface can be calculated from:

$$Q_g = h_g(T_b^g - T_i^g) \quad (5)$$

where h_g is the heat transfer coefficient for the gas boundary layer, in W/m^2/K; T_b^g is the temperature of the bulk gas, in K; T_i^g is the temperature of the gas at the droplet interface, in K.

The derivation of the total heat flux Q is identical to the approach proposed by Zhang *et. al.*[24] The heat transferred though a droplet of radius r can be expressed as:

$$q(r) = \frac{T_i^g(1 - \frac{2\sigma}{H_v^d r\rho}) - T^o}{\frac{1}{4\pi r k_d} + \frac{1}{2\pi r^2 h_i} + \frac{d_w}{4\pi r^2 k_w} + \frac{d_l}{4\pi r^2 k_l}} \quad (6)$$

Where k_d, k_l, k_w represent the thermal conductivities of the droplet which is a mixture of MEG and water, of the insulation layer and of the pipe wall, respectively, in W/m/K; σ is the surface tension of water and MEG mixture, in N/m; H_v^d is the latent heat released from the condensation of MEG and water mixture, in J/kg; ρ is the density of mixture of water and MEG at the droplet interface, in kg/m^3, T^o is the temperature of the outer pipe wall, d_w and d_l are the thickness of the pipe wall and the insulation layer respectively, in m.

The droplet size distribution N(r) can be expressed as:[25]

$$N(r) = \frac{1}{3\pi r^2 r_{max}}(\frac{r}{r_{max}})^{-2/3} \quad (7)$$

The total heat flux (Q) through the droplets to the outside can be then calculated by the integrating the heat flux through single droplets through the entire droplet size distribution per unit area. Eq. (8) yields the final heat balance equation:

$$h_g(T_b^g - T_i^g) + R_{cond}^{water} H_v^{water} + R_{cond}^{MEG} H_v^{MEG} = \int_{r_{min}}^{r_{max}} q(r) N_r dr \quad (8)$$

It can be seen from Eq. (8) that the unknowns are the temperature of the droplet interface T_i^g, the water condensation rate and MEG condensation rate R_{cond}^{water} and R_{cond}^{MEG}. The variables related to the gas or condensed liquid properties can be calculated by taking into account the gas composition and MEG concentration in the condensed liquid. Writing the mass balance provides two additional equations that will enable the calculations of all the variables.

Mass balance

All the water condensing at the top of line comes from the gas phase, so the water condensation rate R_{cond}^{water} can be equated to the mass flux of water through the mass transfer boundary layer:

$$R_{cond}^{water} = \rho_g \beta_g^{water}(y_b^{water} - y_i^{water}) \quad (9)$$

where ρ_g is the gas density, in kg/m^3; β_g^{water} is the mass transfer coefficient of water vapor in the gas, in m/s; y_b^{water} is the mass fraction of water vapor in the bulk gas; y_i^{water} is the mass fraction of water vapor at the gas-liquid interface.

Similarly, the MEG condensation rate R_{cond}^{MEG} can be expressed as:

$$R_{cond}^{MEG} = \rho_g \beta_g^{MEG}(y_b^{MEG} - y_i^{MEG}) \quad (10)$$

where β_g^{MEG} is the mass transfer coefficient of MEG vapor in the gas, in m/s; y_b^{MEG} is the mass fraction of MEG vapor in the bulk gas; y_i^{MEG} is the mass fraction of MEG vapor at the gas-liquid interface.

The mass transfer coefficient of water vapor and MEG vapor can be calculated by:

$$\rho_g \beta_g = \frac{h_g}{C_p} Le^{-2/3} \quad (11)$$

where β_g is the mass transfer coefficient of water or MEG vapor in the gas, in m/s; h_g is the heat capacity of the gas, in J/kg/K; Le is the Lewis number.

Assuming that the liquid phase at the bottom of the pipeline is in equilibrium with the bulk gas phase, the unknown mass fraction of MEG and water vapor in the bulk gas phase can be calculated by using the temperature, pressure and bottom liquid composition. At the top of the line, the gas adjacent the droplet interface equilibrates with the liquid phase at the interface. The bulk gas can be considered as the feeding fluid for the equilibrium at the top of the line, so the compositions of the gas and condensed liquid at the droplet interface can be obtained by performing a flash calculation. Peng-Robinson (PR) equation of state (EoS)[26] with traditional mixing rules is used in this work to calculate the water and MEG fugacity in the gas and liquid phase. The algorithm for flash calculation using equation of state can be found from published literatures.[27,28] After the calculation of the gas and liquid compositions, the gas and liquid properties such as density, heat capacity, thermal conductivity, and mass transfer coefficient as well as heat transfer coefficient can be determined. The minimum and maximum radius of the condensed droplet also can be determined by the methods described by Zhang *et. al*.[24]

Finally, there are three equations (8) - (11), and three unknown variables (R_{cond}^{water}, R_{cond}^{MEG} and T_i^g). By solving these equations, the water and MEG condensation rate can be obtained. The total condensation rate is the summation of water and MEG condensation rate. The MEG content of the condensed liquid at the top of the line is the ratio of MEG condensation rate to the total condensation rate.

Validation of the Co-condensation Model

A large number of water/MEG co-condensation tests were conducted in a large scale flow loop to verify the proposed model predictions. The schematic diagram of the TLC flow loop is shown in Figure 3. The tank is filled with deionized water and MEG and an immersion heater is used to produce the mixture of water and MEG vapors. CO_2 is added to the gas phase and a blower is used for the circulation of the wet gas. The 4" diameter flow loop is 30 meters long and horizontally leveled. The test section is equipped with a cooling system and the temperature of the inner and outer pipe wall can be adjusted by changing the flow rate of the cooling liquid. A thermocouple is used to monitor the gas temperature, while a thermistor inside the pipe wall is used to monitor the pipe wall temperature. A gas/liquid separator is used prior to the test section to redirect the condensed liquid back to the tank. When the hot wet gas contacts the cold pipe wall in the test section, water/MEG co-condensation occurs s and the condensed liquid is drained to a liquid collector located downstream. A transparent quartz column with sale mark is connected to the collector in order to monitor the level of the collected liquid column with time. The accumulation of condensed liquid in the column can be converted to a total condensation rate. The collected condensed liquid is also sampled for analysis of the MEG concentration by gas chromatography.

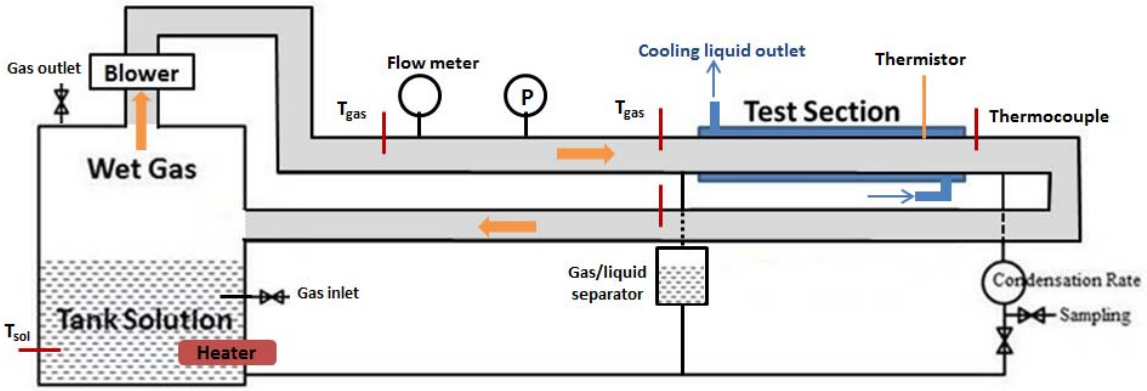

Figure 3: The schematic diagram of the TLC wet gas flow loop.

The ranges of the test parameters for the co-condensation loop tests were listed in Table 1.

Table 1: Test conditions of the co-condensation test in large scale flow loop.

Variables	Range	
	Minimum	Maximum
MEG content in tank solution (wt%)	0	90
Total pressure, P_{total} (bars)	1	3
Gas temperature, T_{gas} (˚C)	42	67
Pipe wall temperature, T_{steel} (˚C)	32	65
Gas velocity, V_{gas} (m/s)	1	3

Figure 4 shows the comparison between the measured total condensation rate (including water and MEG) and the predicted total condensation rate. Because the condensation rates of the tests with 90 wt% MEG in the tank are too small to be seen in the plot in a linear scale, a logarithmic scale is also given. The dotted lines in both plots in Figure 4 represent the ±30% deviation line. The water/MEG co-condensation model gives a good prediction of the condensation rate at MEG free condition, indicating the compatibility of the proposed model with a water-only condensation situation. In the presence of 50 wt% and 70 wt% MEG at the bottom solution, the model predictions agree reasonably well (within 30 %) with the experimental data. However, the calculated condensation rates are significantly lower (one order of magnitude) than the test results for the 90 wt% MEG experiments. The discrepancy is discussed later in the paper.

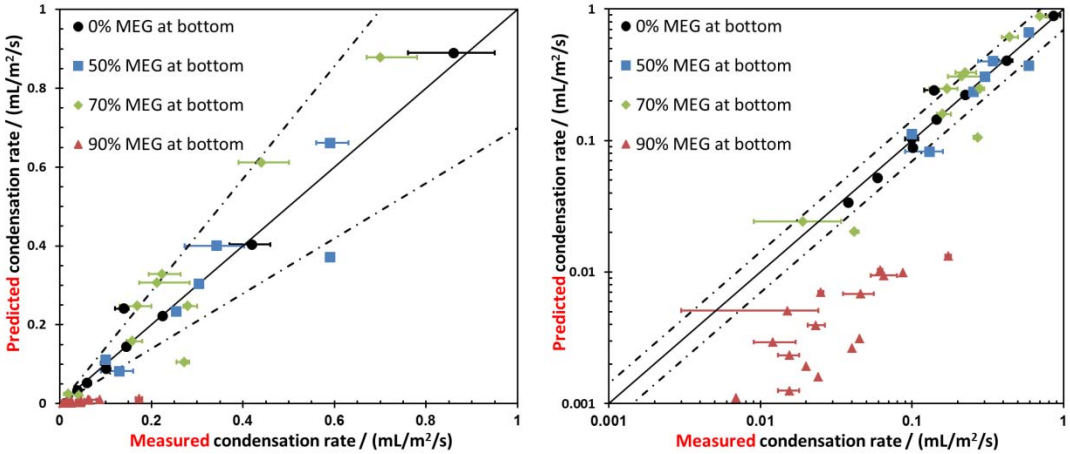

Figure 4: Comparison of the measured and predicted condensation rates.

Figure 5 shows a comparison between the measured MEG concentration in the condensed liquid and the predicted MEG concentration at the top of line. Because most of the 50 wt% and 70 wt% MEG experimental results present a top MEG content lower than 10 wt%, a plot in the logarithmic scale is also given to highlight the deviation of these predictions. The model over predicts the MEG concentration in the condensed phase for most of the conditions. However, both the model predictions and experimental results show that the MEG content at the top of the line is no more than 10 wt% when the MEG content at the bottom of the line is less than 70 wt%.

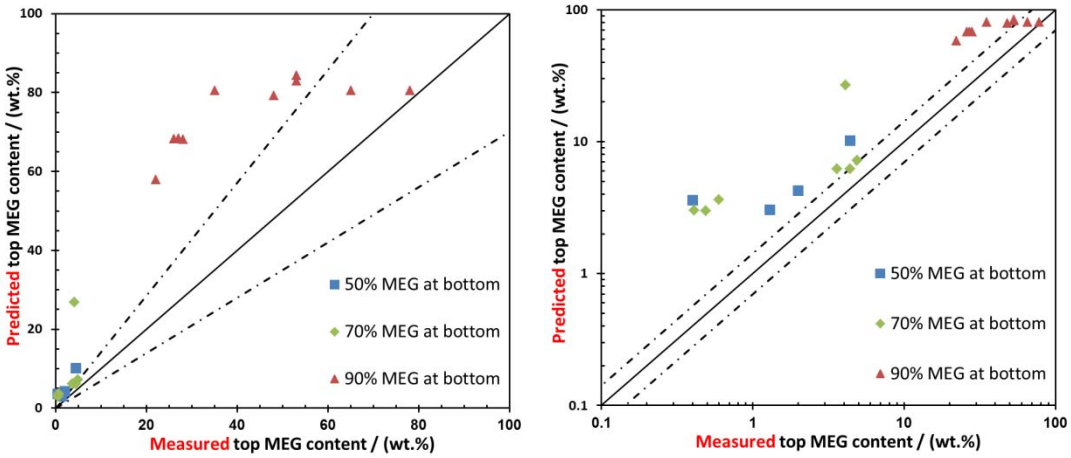

Figure 5: Comparison of the measured and predicted top MEG content.

It is worth noting that the deviation of the model predictions and experiments may be caused by the accuracy of the thermodynamic calculation of gas-liquid phase equilibrium. Folas[29] reported that the Soave-Redlich-Kwong (SRK) EoS using conventional mixing rules over predicted the MEG solubility in wet gas system, while the new developed Cubic-Plus-Association (CPA) EoS and SRK using the Huron-Vidal mixing rule perform satisfactory. Since PR is similar to SRK, the over prediction of top MEG content and corresponding underestimation of condensation rate might be due to the conventional mixing rules. It is also noticed that data of MEG solubility in gas are limited in the literature and their accuracy is questionable.[29] The critical temperature and pressure of MEG and the binary interaction coefficients with other components are not set precisely and several values can be found in the literature.[30-32] The critical temperature and pressure of the components used in this work are listed in Table 2. The binary interaction coefficients are assumed to be 0.

Table 2: Critical temperatures, critical pressures and acentric factors used in the model.

Components	Critical temperature (K)	Critical pressure (bar)	Acentric factor
Water	647.1	219.4	0.343
MEG	720.0	82.0	0.507
Carbon dioxide	304.2	73.9	0.224

The influence of MEG content at the bottom of the line on co-condensation was investigated considering two test conditions. Model predictions and experimental results are compared in Figure 6. The results show clearly that the condensation rate decreases with the increase of the MEG content at the bottom solution. It also can be seen that the MEG concentration of the condensing liquid at the top of the line increases with the MEG content of the bottom solution. However, only a pronounced effect was observed when the MEG content is higher than 70 or 80 wt% at the bottom of the line.

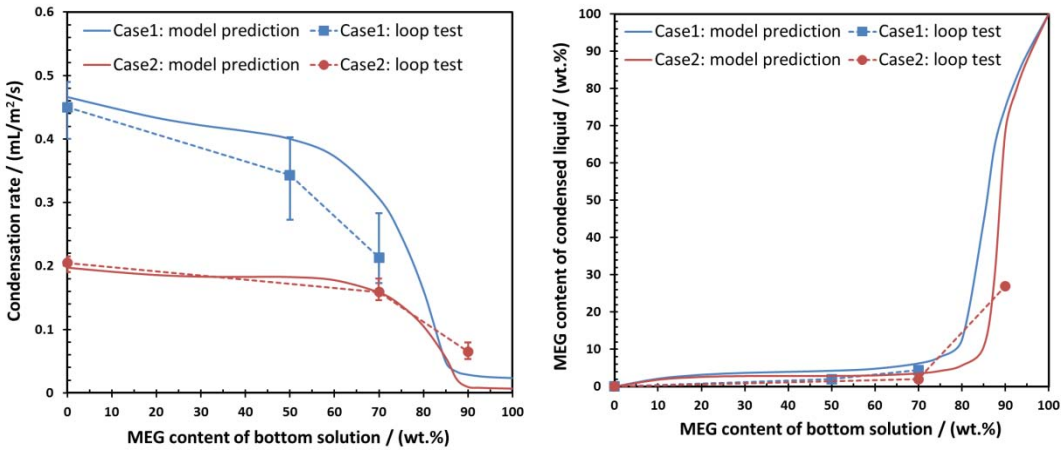

Figure 6: Effect of bottom MEG content on co-condensation, Case 1: T_{gas} = 62 ˚C, T_{steel} = 54 ˚C, P_{total} = 3 bars, V_{gas} = 3 m/s; Case 2: T_{gas} = 42 ˚C, T_{steel} = 34 ˚C, P_{total} = 3 bars, V_{gas} = 3 m/s.

Figure 7 shows the influence of subcooling temperature on the MEG/water co-condensation at different MEG content of the bottom solution. Both the model predictions and experimental results show that the increase of subcooling temperature increases the condensation rate and decreases the MEG content of the condensed liquid at the top of the line. It is also found that, at 5˚C subcooling temperature, a high top MEG content and an extremely low condensation rate can only be obtained when the MEG content at the bottom line is more than 70 wt%. The effect of gas velocity and total pressure were also investigated by model prediction and experiments. As expected, the results shows that the increase of gas velocity increases the total condensation rate while the increase of total pressure slightly decreases the total condensation rate. However, these two factors do not have a great influence on the MEG concentration at the top of the line in the range of conditions tested.

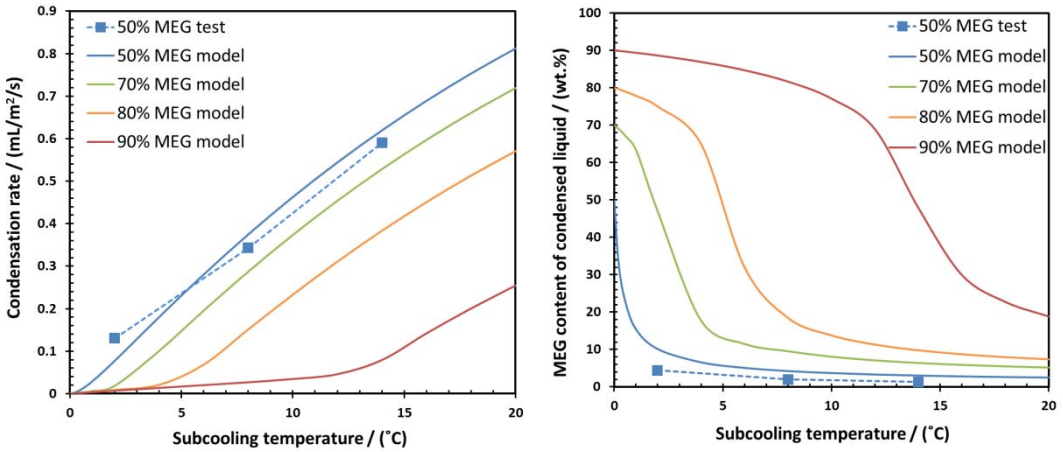

Figure 7: Effect of subcooling temperature ($\Delta T = T_{gas} - T_{steel}$) on the co-condensation, other fixed parameters: T_{gas} = 62 ˚C, P_{total} = 3 bars, V_{gas} = 3 m/s.

Effect of bottom MEG content on TLC

Experimental setup

Long term top of the line corrosion tests with various contents of MEG in the tank solution were performed in the large scale flow loop shown in Figure 3. Pictures of the test section and the weight loss probes are

shown in Figure 8. Three probes with weight loss samples, which are made of API[1] X65 pipeline material, are flush mounted the top of the test section to study the effect of MEG on the corrosion behavior at the top of the line. Before starting the experiments, the whole system is deoxygenated by bubbling CO_2 gas in the tank solution, at the same time the fluid temperature is increased to the desired level. Rather than trying to match the condensation rates between experiments, it was decided instead to control the inner pipe wall temperature. This approach is more effective in capturing the effect of MEG content on the entire process as the condensation and corrosion are in this case closely related. The temperature of the pipe wall is controlled by adjusting the flow rate of the coolant in the copper coil around the test section. After reaching steady state, the weight loss probes sample are installed into the probe ports at the top of test section, and then the test is started.

The weight loss sample surface (except the one exposed to the environment) is coated with a thin layer of electrically insulating polymer coating. The exposed surface of corrosion samples are subsequently grinded with 360, 800 and 1200 grit silicon carbide paper, rinsed with isopropanol and dried before they are mounted to the ports in the test section with specially designed sample holders, as shown in Figure 8 (b). After completion of each test, the weight loss samples surface are prepared for scanning electron microscope (SEM) and cross-section analysis. The corrosion product formed on the sample surface is then removed by exposure to inhibited acid solution (Clarke's solution) to calculate the average corrosion rate by weight loss. Localized corrosion morphology and corresponding pit distribution and depth are obtained by performing a surface analysis on each sample with a 3D surface profilometer.

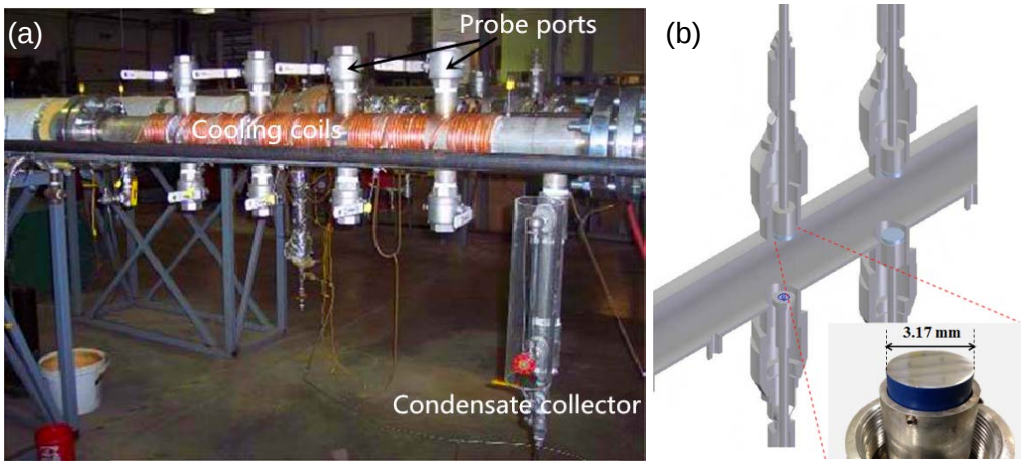

Figure 8: (a) photo of the corrosion test section, (b) weight loss sample and its mounting to the test section.

Influence of 50 wt% MEG ('rich MEG') on TLC

Since 40-50 wt% MEG is the minimum MEG content typically used to prevent the formation of gas hydrate, long term (21 days) top of the line corrosion test with 50 wt% MEG at bottom and without MEG were performed in the flow loop to investigate the 'rich MEG' effect on TLC. It can be seen from Figure 9 that the average corrosion rate with 50 wt.% bottom MEG content is similar to the corrosion rate under MEG free condition. This is in good agreement with the condensation results that showed that 50 wt% MEG has little effect on both condensation rate (decrease of about 24%) and top MEG content (at only 2 wt%). This finding was also reported in Mendez's experimental results.[33] The SEM images indicate that the corrosion product obtained on the steel surface with both MEG free and 50 wt% MEG conditions is $FeCO_3$.

[1] American Petroleum Institute, 1220 L Street, NW Washington, DC 20005-4070

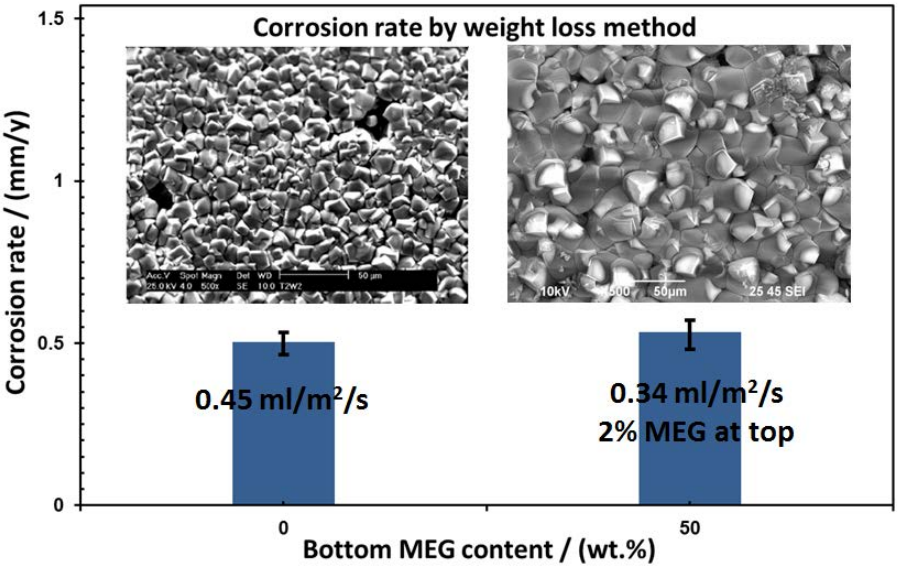

Figure 9: TLC rates, condensation results and SEM surface morphology of corrosion product.

Figure 10 shows the pitting depth distribution of the sample from the 21 days loop test with 50 wt% bottom MEG content. Figure 10a shows the sample surface after the removal of corrosion product layer, which presents signs of localized corrosion. The pitting depth distribution of the sample surface was analyzed using a profilometer as shown in Figure 10. It can be seen that the maximum pitting depth is about 340 μm and its corresponding pitting corrosion rate is 5.2 mm/y. The pitting ratio is also calculated by dividing the maximum pitting corrosion rate to the general corrosion rate. Generally, a high pitting ratio indicates severe pitting corrosion. The pitting ratio is around 10, indicating a clear occurrence of localized corrosion in the presence of 50 wt% MEG at the bottom of line.

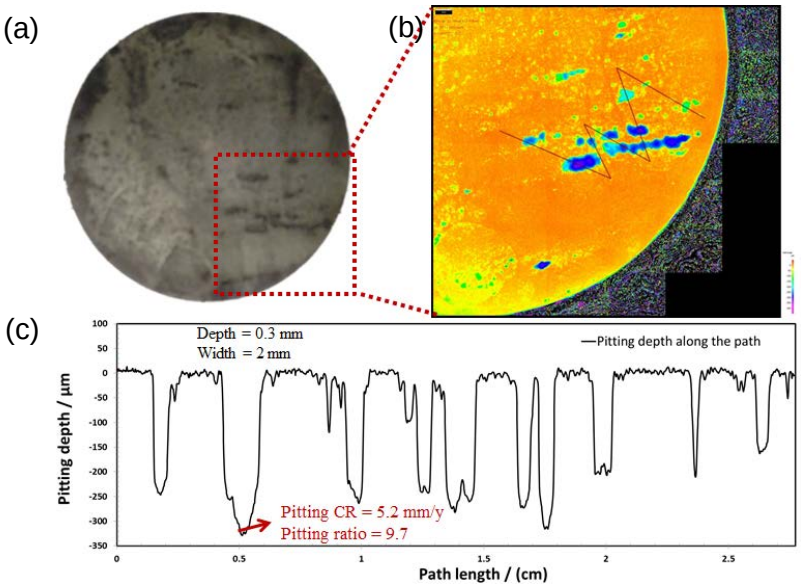

Figure 10: Pitting depth distribution of the sample from the loop test with 50 wt. % MEG at the bottom solution (a) sample morphology after the removal of corrosion film; (b) pitting depth distribution measured by profilometer; (c) pitting depth along the path shown in (b).

In addition, it can also be found that the width of the pits shown in Figure 10c are usually about 10 times bigger than the depth of the corresponding pit, indicating the formation of wide pits with flat bottom. The

characteristic of the pits are confirmed by the SEM images of cross-section view of corrosion product layer at as shown in Figure 11. The pits observed in the SEM images are wide and flat, and their dimensions match the results measured by profilometer.

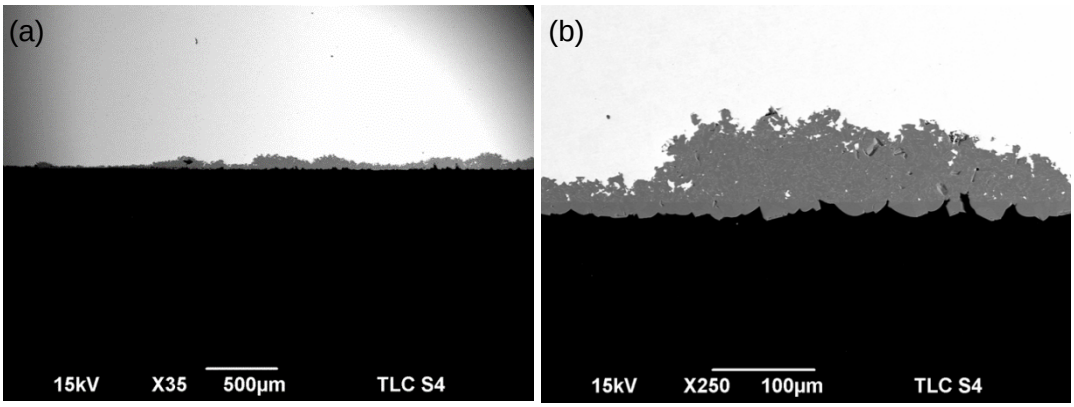

Figure 11: SEM images of cross-sectional view of corrosion product layer at 50 wt% MEG (a) X35, (b) X250.

It should be noted however that similar pitting rates have been measured in the experiment performed in a MEG-free environment. The occurrence of localized corrosion in a TLC scenario is related to a local dissolution of the corrosion product layer due to the constant "refreshing" of the condensed water. This situation is not dependent on the presence or absence of MEG in solution.

Influence of 70 and 90 wt% MEG ('lean MEG') on TLC

Since TLC is more severe at the beginning part of the wet gas pipeline where 'lean MEG' is injected at the well head, the effect of higher MEG content on TLC is also investigated. Table 3 shows the test matrix detailing the experimental conditions of 70 wt% and 90 wt% bottom MEG content flow loop corrosion tests. The results of the average TLC rates, total condensation rate and MEG content of condensing liquid are given in Figure 12 and Figure 13. It can be seen that the TLC rates under both high and low subcooling conditions decreases significantly when the MEG content at bottom increases to 90 wt%. This significant decrease of corrosion rate at 90 wt% MEG can be explained by the strong decrease of the condensation rate and the sharp increase of MEG content at the top of the line, as shown in Figure 13. For the effect of subcooling temperature, higher TLC rates were obtained at higher subcooling temperature from both 70 wt% and 90 wt% bottom MEG content, which can be attributed to the changes of condensation rate and top MEG content.

Table 3: Matrix of 70 and 90 wt% MEG flow loop corrosion tests.

Parameters	70 wt% and 90 wt% MEG corrosion tests			
MEG content in tank solution (wt%)	70	90	70	90
Total pressure, P_{total} (bars)	3			
Gas velocity, V_{gas} (m/s)	3			
Exposure time, t (day)	21			
Gas temperature, T_{gas} (˚C)	42			
Pipe temperature, T_{wall} (˚C)	34		40	
Subcooling temperature, ΔT (˚C)	High ΔT		Low ΔT	

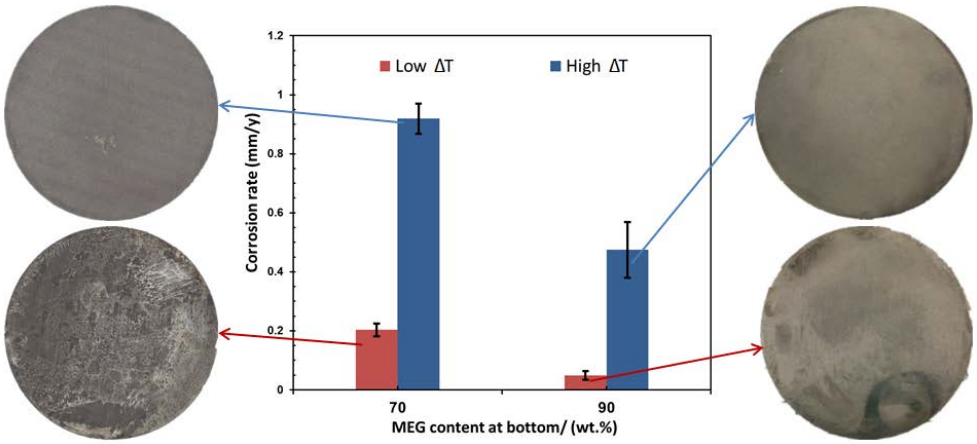

Figure 12: Corrosion rates and sample photos after the removal of corrosion product at different bottom MEG contents and subcooling temperatures (∆*T*).

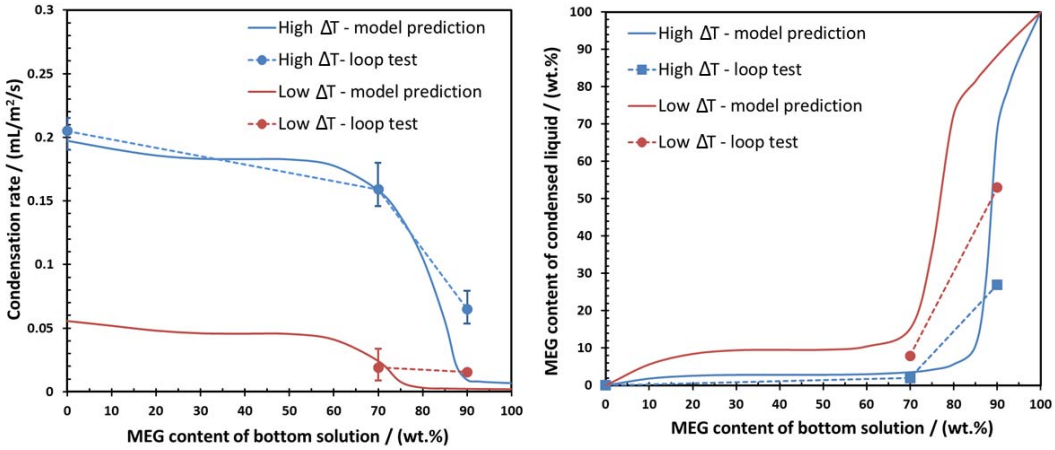

Figure 13: Co-condensation results at different bottom MEG contents and subcooling temperatures (∆*T*).

Inspection of the 90wt% MEG test samples after removal of the corrosion product layer only showed a morphology typical of uniform corrosion. In contrast, the samples taken from the 70 wt% MEG tests displayed signs of extensive localized corrosion, both for low and high subcooling. The localized corrosion morphology at 70 wt% MEG was analyzed with a 3D profilometer, as shown in Figure 14. Pitting rates of 1.5 to 2.6 mm/y were measured with high pitting ratio observed for the lower subcooling condition.

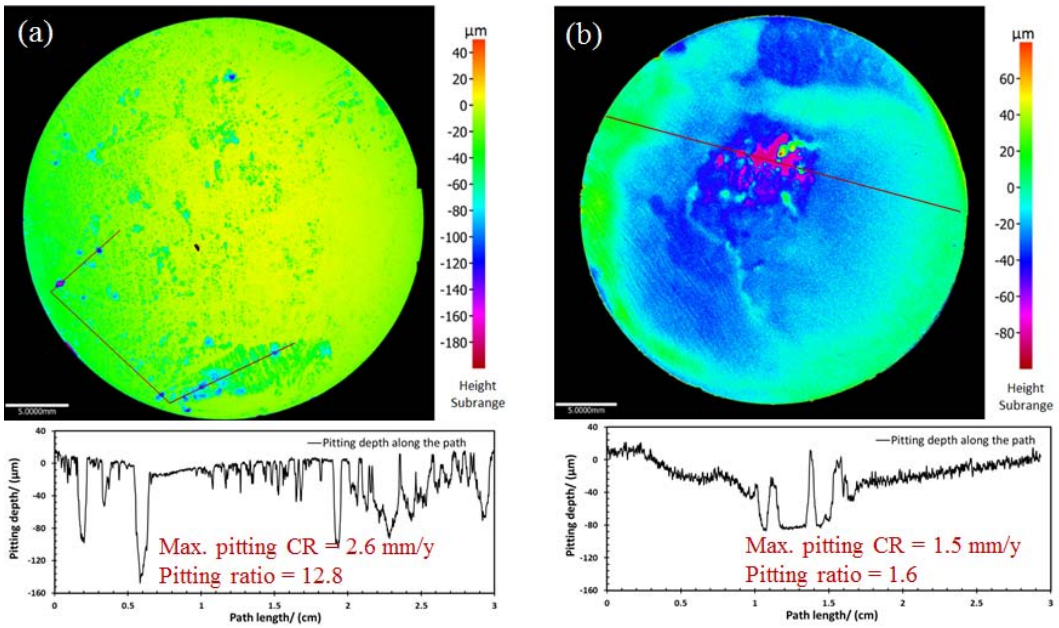

Figure 14: Pitting depth distribution for 70 wt% MEG loop tests (a) low ΔT section; (b) high ΔT section.

Figure 15 shows the SEM images of the steel surface and of a cross-section of the corrosion product layer obtained during the 70 wt% bottom MEG content experiment. For low subcooling condition, the corrosion product layer appears dense but some gaps can also be observed between adjacent crystalline grains, as shown in Figure 15a. The SEM cross-section (Figure 15b) shows clear areas of bare steel within the pit as a sign of high penetration rates. For high subcooling condition, a porous corrosion product layer is observed, displaying a large gap between the layer and the steel surface. Corrosion could easily occur underneath such a non-protective corrosion product layer.

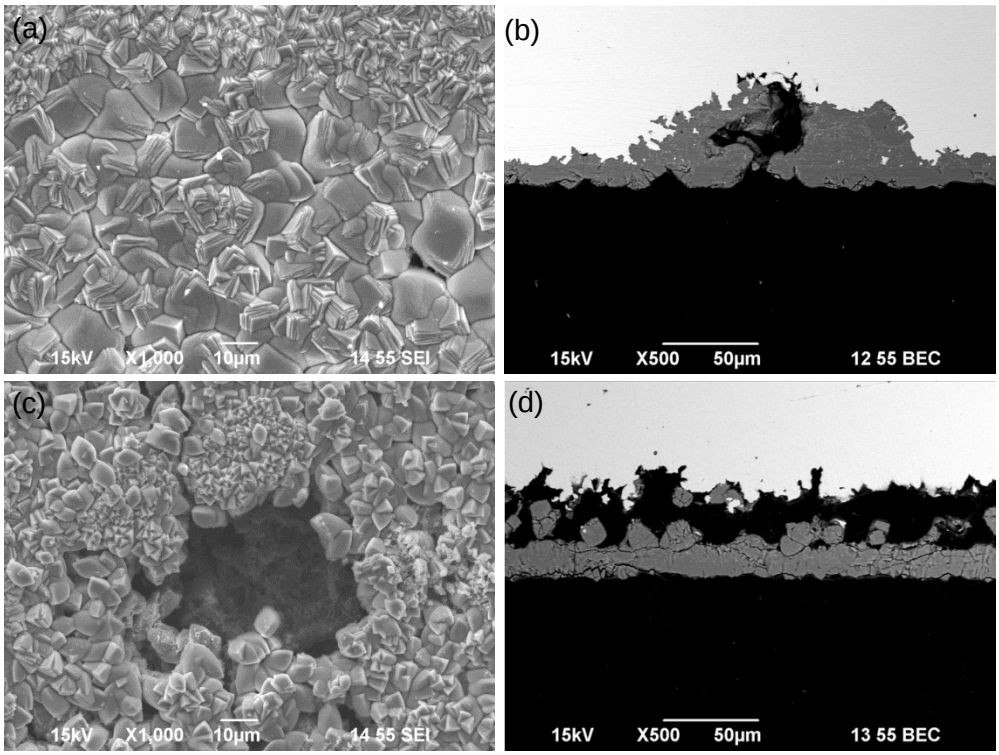

Figure 15: SEM images of corrosion product layer from 70 wt% bottom MEG content loop test, (a) and (b) low ΔT section; (c) and (d) high ΔT section.

Figure 16 shows the SEM images of surface and cross-sectional views of the corrosion product layer considering the 90 wt% MEG experiment. In general, the corrosion product layer seems thinner (10 to 20 μm) but compact and adherent to the steel surface. Although a few gaps within the layer and between the layer and the steel surface could be observed, (Figure 16b and d), no localized corrosion was identified. Therefore, the absence of localized corrosion at 90 wt% bottom MEG content may be due to the decrease of condensation rate and increase of top MEG content, along with an improvement of the corrosion product layer protectiveness.

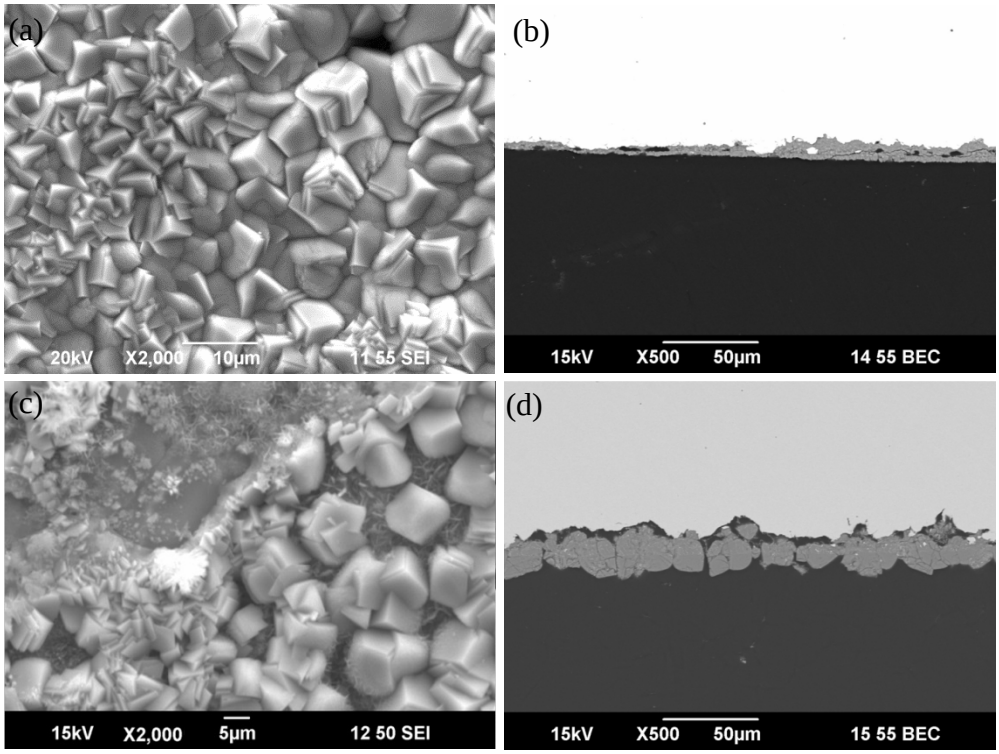

Figure 16: SEM images of corrosion product layer from 90 wt% bottom MEG content loop test, (a) and (b) low ΔT section; (c) and (d) high ΔT section.

CONCLUSIONS

A mechanistic model is developed to predict the co-condensation of MEG and water in CO_2 environment. The predictions are in good agreement with experimental results performed in flow loop.

The increase of the MEG content at the bottom of the line does not only decrease the total condensation rate, but also increase the MEG content of condensing phase at the top of the line.

A pronounced effect on condensation rate and top MEG content is observed when the MEG content is higher than 70-80 wt% at the bottom of the line.

The addition of 50 wt% and 70 wt% MEG at the bottom solution has little effect on TLC rate. In these conditions, the top MEG content is always less than 10 wt%. Pitting corrosion could be observed although it is a typical occurrence even win the absence of MEG.

The presence of 90 wt% MEG at the bottom liquid phase decreases the TLC rate significantly because of the sharp decrease of condensation rate and increase in MEG content in the condensing phase (up to 53 wt%). No localized corrosion was observed in the presence of 90 wt% MEG.

ACKNOWLEDGEMENTS

The authors would like to thank the following companies for their financial support: Apache, BHP Billiton, BP, Chevron, ConocoPhillips, MI-SWACO, PETRONAS, PTTEP, Woodside and Talisman.

REFERENCES

[1] D. Hinkson, Z. Zhang, M. Singer, S. Nesic, "Chemical Composition and Corrosivity of the Condensate in Top-of-the-Line Corrosion" Corrosion, 64, 4(2010): 045002-1-045002-8

[2] P.C. Okafor, S. Nesic, "Effect of Acetic acid on CO_2 Corrosion of Carbon Steel in Vapor-Water Two-Phase Horizontal Flow", Chemical Engineering Communications, 194, (2007): 141-157.

[3] T.R. Andersen, A.M.K. Halvorsen, A. Valle, G.P. Kojen, "The Influence of Condensation rate and Acetic acid concentration on TOL-Corrosion in Multiphase pipelines", CORROSION/2007, paper no. 312 (Houston, TX: NACE, 2007).

[4] A. Camacho, M. Singer, B. Brown, S. Nesic, "Top of the Line Corrosion in H_2S/CO_2 Environments", CORROSION/2008, paper no. 470 (Houston, TX: NACE, 2008).

[5] M. Singer, S. Nesic, Y. Gunaltun, "Top of the Line Corrosion in Presence of Acetic Acid and Carbon Dioxide", CORROSION/2004, paper no. 377 (Houston, TX: NACE, 2004).

[6] F. Vitse, S. Nesic, Y. Gunaltun, D. Larrey de Torreben, P. Duchet-Suchaux, "Mechanistic Model for the Prediction of Top-of-the-Line Corrosion Risk", Corrosion, 59, 12(2003): 1075-1084.

[7] M. Singer, D. Hinkson, Z. Zhang, H. Wang, S. Nesic, "CO_2 Top-of-the-Line Corrosion in Presence of Acetic Acid: A Parametric Study", 69, 7(2013): 719-735.

[8] K.S. Pedersen, M.L. Michelsen, A.O. Fredheim, "Phase equilibrium calculations for unprocessed well streams containing hydrate inhibitors", Fluid Phase Equilibria, 126, (1996): 13-28.

[9] G. Svenningsen, R. Nyborg, "Modeling of Top of Line Corrosion with Organic Acid and Glycol", CORROSION/2014, paper no. 4057 (Houston, TX: NACE, 2014).

[10] J-L. Crolet, J-P. Samaran, "The use of the anti-hydrate treatment for the prevention of CO_2 corrosion in long crude gas pipelines" CORROSION/93, paper no. 102 (Houston, TX: NACE, 1993).

[11] L. van Bodegom, K. van Gelder, M.K.F. Paksa, L. van Raam, "Effect of Glycol and Methanol on CO_2 Corrosion of Carbon Steel", CORROSION/87, paper no. 55 (Houston, TX: NACE, 1987).

[12] L. van Bodegom, K. van Gelder, J.A.M. Spaninks, "Control of CO_2 Corrosion in Wet Gas Lines by Injection of Glycol", CORROSION/88, paper no. 187 (Houston, TX: NACE, 1988).

[13] C. deWaard, U. Lotz, D.E. Milliams, "Predictive Model for CO_2 Corrosion Engineering in Wet Natural Gas Pipelines", Corrosion, 48, 17(1993): 976-985

[14] E. Gulbrandsen, J-H. Morard, "Why does Glycol Inhibit CO_2 Corrosion?", CORROSION/98, paper no. 221 (Houston, TX: NACE, 1998).

[15] T. Pojtanabuntoeng, M. Salasi, R. Gubner, "The Influence of Mono Ethylene Glycol (MEG) on CO_2 Corrosion of Carbon Steel at Elevated Temperature (80 to 120 °C)", CORROSION/2014, paper no. 4176 (Houston, TX: NACE, 2014).

[16] W. Hayduk, V.K. Malik, "Density, Viscosity, and Carbon Dioxide Solubility and Diffusivity in Aqueous Ethylene Glycol Solutions", Journal of Chemical and Engineering Data, 16, 2(1971):143-146.

[17] M.H. Oyevaar, R.W.J. Morsslnkhof, K.R. Westerterp, "Density, Viscosity, Solubility, and Diffusivity of CO_2 and N_2O in Solutions of Diethanolamine in aqueous Ethylene Glycol at 298 K", Journal of Chemical and Engineering Data, 34, (1989): 77-82.

[18] H. Hu, A.T. Kan, M.B. Tomson, "Effects of Monoethylene Glycol on Carbonate Equilibrium and Calcite Solubility in Gas/Monoethylene Glycol/NaCl/Water Mixed Systems", SPE Journal, 15, 3(2010):714-725.

[19] J.N.J.J. Lammers, "Phase Behavior of Glycol in Gas Pipeline Calculated", Oil and Gas Journal, 89, (1991):15.

[20] B.F.M. Pots, E.L.J.A. Hendriksen, "CO_2 Corrosion under Scaling Conditions – The Special Case of Top-of-Line Corrosion in Wet Gas Pipelines", CORROSION/2000, paper no. 31 (Houston, TX: NACE, 2000).

[21] J.T. Schrodt, “Simultaneous Heat and Mass Transfer from Multicomponent Condensing Vapor-Gas Systems”, AlChE Journal, 19, 4(1973): 753-759.
[22] Y.M. Gunaltun, D. Supriyataman, J. Achmad, “Top-of-the-Line Corrosion in Multiphase Gas Lines: A Case History”, CORROSION/99, paper no. 36 (Houston, TX: NACE, 1999).
[23] Y.M. Gunaltun, D. Larrey, “Correlation of Cases of Top-of-Line Corrosion with Calculated Water Condensation Rates”, CORROSION/2000, paper no. 71 (Houston, TX: NACE, 2000).
[24] Z. Zhang, D. Hinkson, M. Singer, H. Wang, S. Nesic, “A Mechanistic Model of Top-of-the-Line Corrosion”, Corrosion, 63, 11(2007): 1051-1062.
[25] J.W. Rose, L.R. Glicksman, “Dropwise Condensation – The Distribution of Drop Sizes”, International Journal of Heat and Mass Transfer, 16, (1973): 411-425.
[26] D-Y. Peng, B. Robinson, “A New Two-Constant Equation of State”, Industrial & Engineering Chemistry Fundamentals, 15, 1(1976): 59-64.
[27] D. Veeranna, A. Husain, “An Algorithm for Flash Calculations Using an Equation of State”, Computers & Chemical Engineering, 11, 5(1987): 489-496.
[28] H.S. Naji, “Conventional and Rapid Flash Calculations for the Soave-Redlich-Kwong and Peng-Robinson Equation of State”, Emirates Journal for Engineering Research, 13, 3(2008): 81-91.
[29] G.K. Folas, O.J. Berg, E. Solbraa, A.O. Fredheim, G.M. Kontogeorgis, M.L. Michelsen, E.H. Stenby, “High-pressure Vapor-liquid Equilibria of Systems Containing Ethylene Glycol, Water and Methane Experimental measurements and modeling”, Fluid Phase Equilibria, 251 (2007): 52-58.
[30] E.D. Nikitin, P.A. Pavlov, P.V.Skripov, “Measurement of the Critical Properties of Thermally Unstable Substances and Mixtures by the Pulse-heating Method”, The Journal of Chemical Thermodynamics, 25, (1993): 869-880.
[31] D. Zheng, W. Ma, R. Wei, T. Guo, “Solubility Study of Methane, Carbon Dioxide and Nitrogen in Ethylene Glycol at Elevated Temperatures and Pressures”, Fluid Phase Equilibria, 155, (1999): 277-286.
[32] L. Zhang, W. Wu, Y. Sun, L. Li, B. Jing, X. Li, N. Yang, H. Ding, “Isobaric Vapor-Liquid Equilibria for the Binary Mixtures Composed of Ethylene Glycol, 1,2-Propylene Glycol, 1,2-Butanediol, and 1,3-Butanediol at 10.00 kPa”, Journal of Chemical & Engineering Data, 58, (2013): 1308-1315.
[33] C. Mendez, M. Singer, A. Camacho, S. Hernandez, S. Nesic, “Effect of Acetic Acid, pH and MEG on the CO_2 Top of the Line Corrosion”, CORROSION/2005, paper no. 278 (Houston, TX: NACE, 2005).